J. Water Environ. Nanotechnol., 7(3): 230-240 Summer 2022

ORIGINAL RESEARCH PAPER

Innovative synthesis of TiO_2 nanorod/WO_3 nanoflakes heterojunction photocatalyst for visible light degradation of Nitenpyram insecticide

Ghader Hosseinzadeh

Department of Chemical Engineering, University of Bonab, Bonab, Iran.

Received: 2022-04-28 Accepted: 2022-06-15 Published: 2022-07-01

ABSTRACT

In the current study, for the first time, an innovative hydrothermal method was proposed for the synthesis of TiO_2/WO_3 heterojunction nanocomposite from the combination of TiO_2 nanorod, and WO_3 nanoflakes. Because of environmental issues arising from the vast use of insecticides, this nanocomposite photocatalyst was applied for the first time for photocatalytic degradation of Nitenpyram insecticide under visible light irradiation. The prepared nanocomposite was fully characterized by XRD, FESEM, DRS, PL, and Mott-Schottky analysis. The results revealed that the heterojunction sample had the best photocatalytic performance. The enhanced photocatalytic activity of this heterojunction is attributed to the decrease of the charge carrier's recombination rate and enhanced visible light harvesting. Moreover, based on the radical trapping experiments and Mott-Schottky calculations, hydroxide radical was determined as the main active species for decomposition of Nitenpyram insecticide, and type II charge transfer mechanism was revealed to be responsible for the enhanced photocatalytic performance, which charge transfer between the two semiconductors results in the decreasing of the charge carrier's recombination rate.

Keywords: *TiO_2, WO_3, Heterojunction, Photocatalyst, Nitenpyram*

How to cite this article

Hosseinzadeh Gh. Innovative synthesis of TiO_2 nanorod/WO_3 nanoflakes heterojunction photocatalyst for visible light degradation of Nitenpyram insecticide. J. Water Environ. Nanotechnol., 2022; 7(3): 230-240.

DOI: 10.22090/jwent.2022.03.001

INTRODUCTION

Nowadays, various insecticides are widely used in agriculture, and their subsequent release into the environment such as groundwater, rivers, and soil creates serious environmental problems [1]. Nitenpyram, as an effective neonicotinoid, is one of the most commonly used insecticides [2]. Recently developed techniques for removing insecticides from polluted environments are biodegradation, membrane reactors, hybrid adsorption/coagulation/flocculation, catalytic hydrolysis, and advanced oxidation process (AOP) [3-7]. Among these methods, AOP by using semiconductor photocatalysts is a promising technology for the decomposition of organic pollutants in environmental remediation applications [8].

In recent decades, titanium dioxide (TiO_2), as an n-type semiconductor, has gained much consideration in the photocatalytic processes due to its interesting features such as good physicochemical stability, low cost, high oxidation power of photoinduced electrons and holes, stability and reusability [9]. However, because of the fast recombination of the photoinduced electron-hole pairs, and low sunlight harvesting ability, the photocatalytic performance of bare TiO_2 is rather low [10]. Based on the above considerations, various methods have been developed to overcome the restrictions of TiO_2 such as doping with metal or nonmetal elements [11], compositing with graphene or g-C_3N_4 [12-14], engineering its morphology

* Corresponding Author Email: *g.hosseinzadeh@ubonab.ac.ir*

and surface structure[15, 16], and heterojunction formation with other semiconductors [17, 18]. Currently, as a promising approach, a combination of a semiconductor with a second semiconductor in the form of a heterojunction photocatalyst has attracted much attention, which leads to the efficient separation of the photoinduced electron-hole pairs and improvement of the sunlight absorbance efficiency[19, 20].

Tungsten oxide (WO_3), as an n-type transition metal Oxide semiconductor with a suitable band gap energy of ~2.5 eV for visible light absorption has been widely used in a wide range of photocatalytic applications [21]. This is because of its excellent features such as suitable valence and conduction band position, high visible light absorption, good stability, low cost, and outstanding electrochemical and optical properties [22-25]. However, because of its narrow band gap, and fast charge carriers' recombination rate, this semiconductor has low photocatalytic efficiency [26]. In this regards various strategies have been developed to the improvement of its photocatalytic efficiency, including compositing with carbon nanostructures [27, 28], doping with other elements [29, 30], surface engineering [31, 32], and hybridization with other semiconductor photocatalysts in heterojunction nanocomposites [33]. Among these methods, the heterojunction photocatalysts are promising and different heterojunction nanocomposites of WO_3 were synthesized such as WO_3/TiO_2 [34], $WO_3/BiVO_4$ [35], WO_3/ZnO [36], WO_3/Bi_2O_3 [37], and WO_3/AgBr [38].

Although, there are some articles about TiO_2/WO_3 nanocomposite photocatalyst [39, 40], however, for the first time in the current study, a TiO_2/WO_3 heterojunction nanocomposite was synthesized through hydrothermal technique from novel morphology of TiO_2 nanorod, and WO_3 nanoflake. The nanocomposite was applied for photocatalytic degradation of Nitenpyram insecticide under visible light irradiation, for the first time. The as-prepared composite was fully characterized by XRD, FESEM, DRS, PL, and Mott-Schottky analysis. Furthermore, based on the optical, photoelectrochemical and photocatalytic activity test results, a possible charge transfer mechanism was proposed.

EXPERIMENTAL

Materials

Titanium isopropoxide, HCl, NaOH, Triethanolamine, ethanol, $Na_2WO_4.2H_2O$, L-lysine, Nitenpyram, tert-Butyl alcohol, benzoquinone, and Ethylenediaminetetraacetic acid were purchased in analytical grade from Merck, Germany, and were used as raw materials without any purification.

Synthesis of TiO_2 nanorods

TiO_2 nanorods were prepared by hydrothermal method. Briefly, 3.5 ml of Titanium isopropoxide was mixed with 7 ml of Triethanolamine, then this mixture was fully dissolved in 50 ml of deionized water by magnetic stirring. The final solution was poured into a Teflon-lined stainless autoclave and maintained at 180 °C for 20 h. The obtained precipitate was separated by centrifuging at 5000 rpm and washed several times with distilled water and dried at 80 °C.

Synthesis of WO_3 nanoflakes

WO_3 nanoflakes were also prepared by hydrothermal method. For this purpose, 0.75 g of $Na_2WO_4.2H_2O$ was mixed with 1.5 g of L-lysine and after adjusting the pH to 1 by 4 M HCl solution the final mixture was dissolved in 40 ml of deionized water under magnetic stirring. The final solution was transferred into a 75 ml Teflon-lined stainless autoclave and maintained at 170 °C for 12h. The final precipitates were immediately separated by centrifugation, washed several times with distilled water and ethanol, and dried at 80 °C.

Synthesis of TiO_2/WO_3 nanocomposite

For the synthesis of TiO_2/WO_3 nanocomposite, containing 40% (w/w) WO_3 and 60% (w/w) TiO_2, in a typical process, 0,6 g WO_3 nanoflakes were fully dispersed in 50 ml deionized water by probe ultrasonication, then 3.5 ml of Titanium isopropoxide and 7 ml of Triethanolamine were dissolved in above suspension by magnetic stirring. The final suspension was poured into a Teflon-lined stainless autoclave and maintained at 180 °C for 20h. The resulting nanocomposite was separated by centrifugation, washed several times with distilled water and ethanol, and dried at 80 °C.

Characterizations

The crystal characteristics of the obtained photocatalysts were analyzed by X-ray diffraction (XRD) on Philips X' Pert MPD with Cu Kα radiation (λ= 0.15406 nm) in 2θ range from 10° to 80°. MIRA3 TESCAN field emission scanning electron microscopy (FESEM) was applied to

investigate the morphology and particle size of the photocatalyst samples. Diffuse reflectance spectroscopy (DRS) in the region of 200 to 800 nm was performed by means of a Shimadzu UV-2550 UV–vis spectrophotometer. Varian Cary-Eclipse 500 fluorescence spectrometer was used to obtain the photoluminescence (PL) spectra of samples at an excitation wavelength of 300 nm. Photo-electrochemical characteristics of the samples were assessed using a Gamry potentiostat in a conventional three-electrode system of Ag/AgCl (reference electrode), Pt foil (counter electrode), and the prepared samples (as a working electrode) in 0.1 M aqueous solution of Na_2SO_4 as electrolyte and under irradiation of 570 W Xenon lamp equipped with L41 UV-cut off filter (Kenko Co.).

Photocatalytic activity

The photocatalytic efficiencies of the synthesized samples were investigated by measuring the degradation percentage (D.P.) of Nitenpyram insecticide under visible light irradiation. A 570W Xenon lamp equipped with an L41 UV-cut-off filter (Kenko Co.) was used as a visible light source. Briefly, 30 mg of photocatalyst sample was fully dispersed in 100 mL of the wastewater. The resulting suspension was maintained under dark conditions and stirred for 2 h to reach an adsorption-desorption equilibrium, and afterward was irradiated. Every 15 min, 5 mL of aliquot was sampled and immediately centrifuged to deposit the remnant photocatalyst nanocomposites, and the remaining concentration of Nitenpyram insecticide was measured by Cary 100 Bio UV–Vis spectrophotometer at its maximum wavelengths of 218 nm.

RESULTS AND DISCUSSION

XRD

The XRD patterns of the prepared samples were illustrated in Fig. 1. For the TiO_2 sample, the main peaks at 2θ of 25.2, 37.7, 48.0, 53.8, and 54.8° are respectively assigned to the (101), (004), (200), (105), and (211) crystal planes of TiO_2 with anatase structure (JCPDS 21-1272) [41]. In the XRD pattern of WO_3, the major diffraction peaks positioned at 2θ of 13.9°, 22.7°, 26.8°, 28.2°, and 36.5° can be respectively indexed to the (100), (001), (101), (200), and (201) diffraction planes of the hexagonal WO_3 with JCPDS #33-1387 [42]. In the diffraction patterns of the TiO_2-WO_3 sample, the characteristic diffraction peaks of both WO_3 and TiO_2 are present, which indicates the successful synthesis of the nanocomposite TiO_2-WO_3 sample. The broadening of the diffraction peaks demonstrates the nanostructure nature of the prepared samples.

FE-SEM

The FE-SEM images were taken from the WO_3, TiO_2, and TiO_2-WO_3 samples to characterize their morphology and particle size. The results of FE-

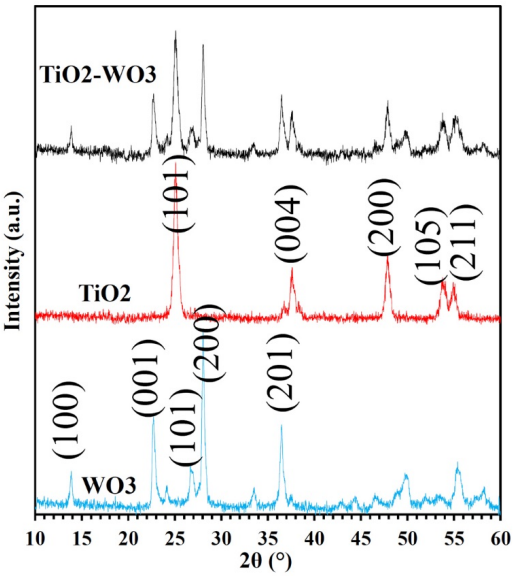

Fig. 1. XRD patterns of the prepared samples.

SEM images for the samples prepared are given in Fig. 2. Fig. 2(A) demonstrates the FE-SEM image of the TiO_2 sample, as seen, this sample contains the TiO_2 nanorods with an approximate diameter of 40 nm and an approximate length of 150 nm. Based on the FE-SEM image of the WO_3 sample (Fig. 2(B)), this sample is made up of the WO_3 nanoflakes with a thickness of approximately 30 nm. In the FE-SEM image of the TiO_2-WO_3 nanocomposite (Fig. 2(C)), both the TiO_2 nanorods and the WO_3 nanoflakes are seen. Furthermore, the suitable distribution of the TiO_2 nanorods on the WO_3 nanoflakes is observed in this image.

DRS

In order to evaluate the photocatalytic performance of a photocatalyst, its optical behavior must be examined. To study the photo-response characteristics of the prepared samples, the light absorption spectra of the prepared samples were tested by UV-Vis diffuse reflectance spectroscopy (UV-DRS), and the relevant results are shown in Fig. 3. As is seen in Fig. 3(A), the absorption edges of the WO_3, TiO_2, and TiO_2-WO_3 samples are found to be around 460, 395, and 420 nm, respectively. As can be seen, anatase TiO_2 nanorods

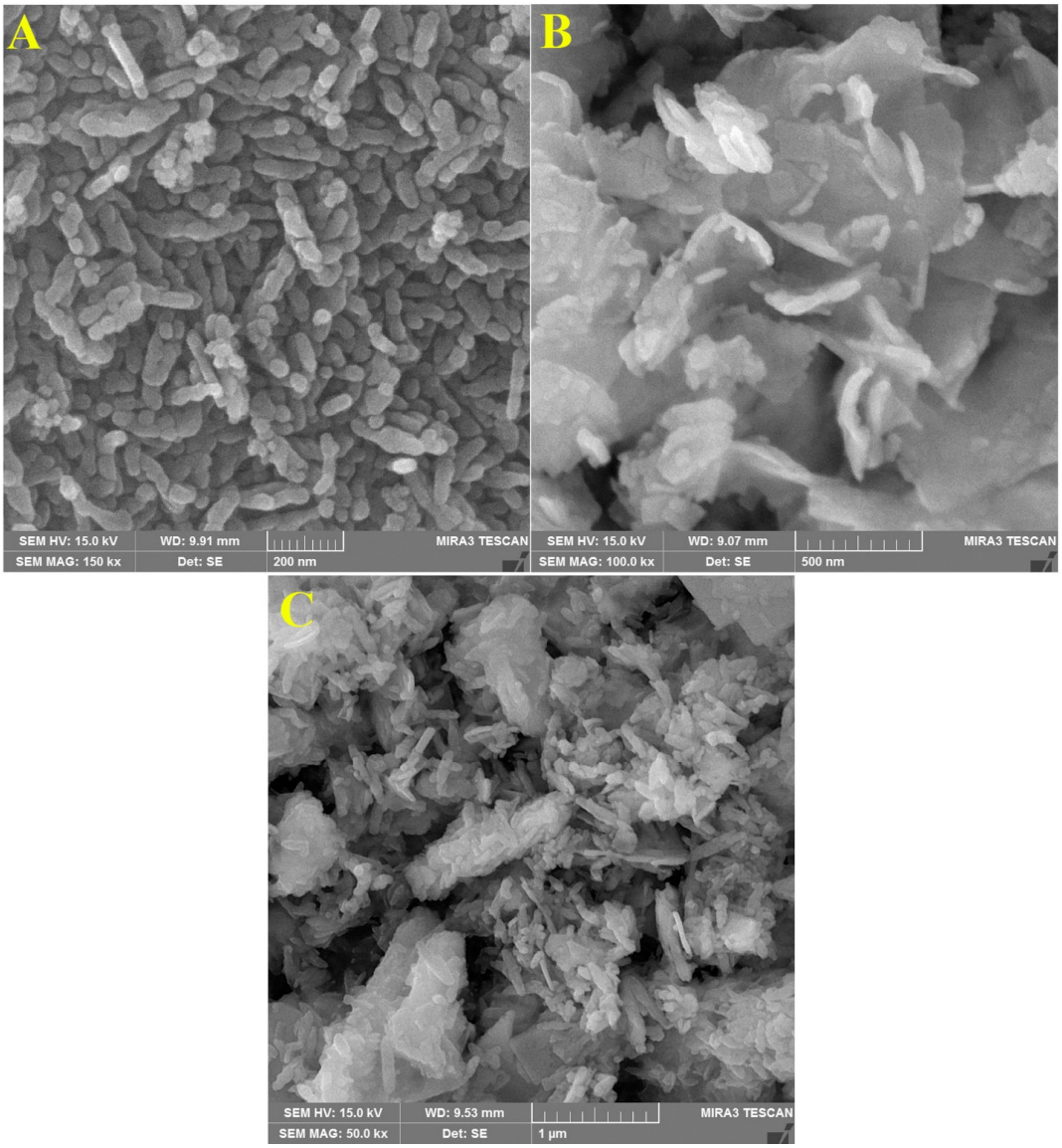

Fig. 2. FE-SEM images of TiO_2 (A); WO_3 (B) and TiO_2-WO_3 heterojunction nanocomposite (C).

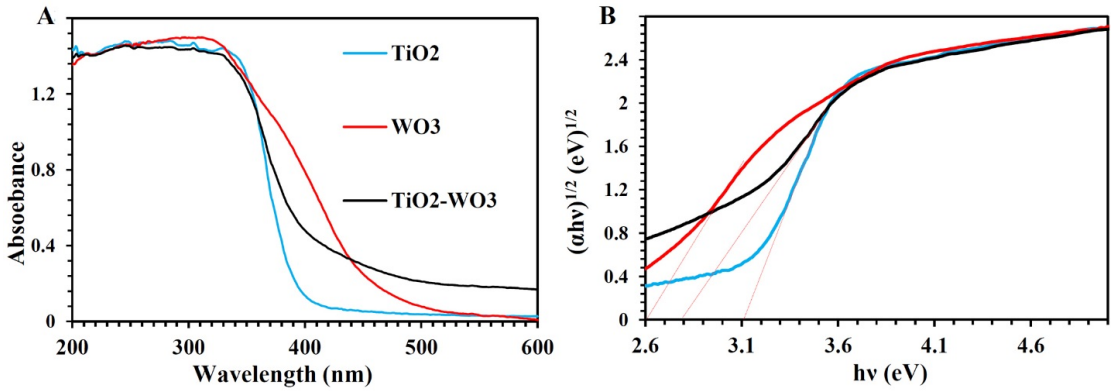

Fig. 3. (a) UV-Vis diffuse reflectance and (b) Tauc plots for the corresponding samples.

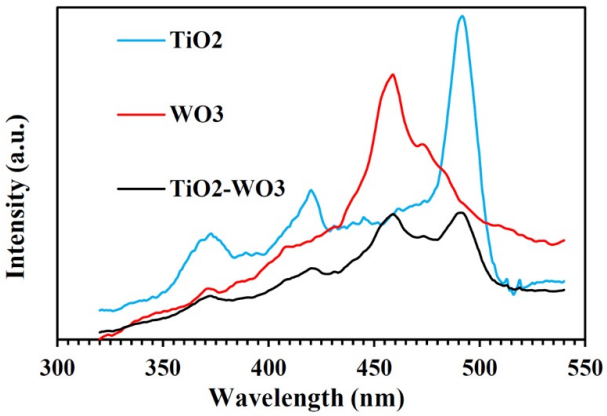

Fig. 4. PL spectra of the prepared samples.

mainly absorb ultraviolet light. WO_3, on the other hand, tends to absorb visible light radiation. The presence of WO_3 in the structure of TiO_2 shifts the TiO_2 absorption edge towards the visible light region, which can improve the photocatalytic performance of the nanocomposite sample under visible light radiation. In order to study this effect more precisely, the band gap energy of the samples was examined based on the Tauc formula [43]. As shown in (Fig. 3(B)) the band gap energies of the WO_3, TiO_2, and TiO_2-WO_3 samples are 2.6, 3.1, and 2.8 eV, respectively. Therefore heterojunction formation between TiO_2 and WO_3 remarkably decreases the band gap energy of TiO_2, which could result in an improvement of photocatalytic activity under solar light irradiation.

Photoluminescence (PL)

The separation of charge carriers, i.e. photoinduced electrons and holes, is one of the effective factors in the photocatalytic performance of a photocatalyst sample. 3.4. Photoluminescence (PL) spectroscopy can be used to study the effect of heterojunction formation between TiO_2 and WO_3 semiconductors on the separation and transportation of charge carriers in the TiO_2-WO_3 heterojunction sample. In this case, any decrease in the PL intensity indicates a decrease in the electron-hole recombination which can result in the improvement of the photocatalyst performance [44]. As can be seen in Fig. 4, the PL intensity of the TiO_2-WO_3 nanocomposite is remarkably lower than that of the TiO_2 and WO_3 samples, so it can be concluded that heterojunction formation between TiO_2 and WO_3 effectively reduced the electron-hole recombination. Therefore, the TiO_2-WO_3 sample could have improved photocatalytic activity due to the diminished charge carriers' recombination rate.

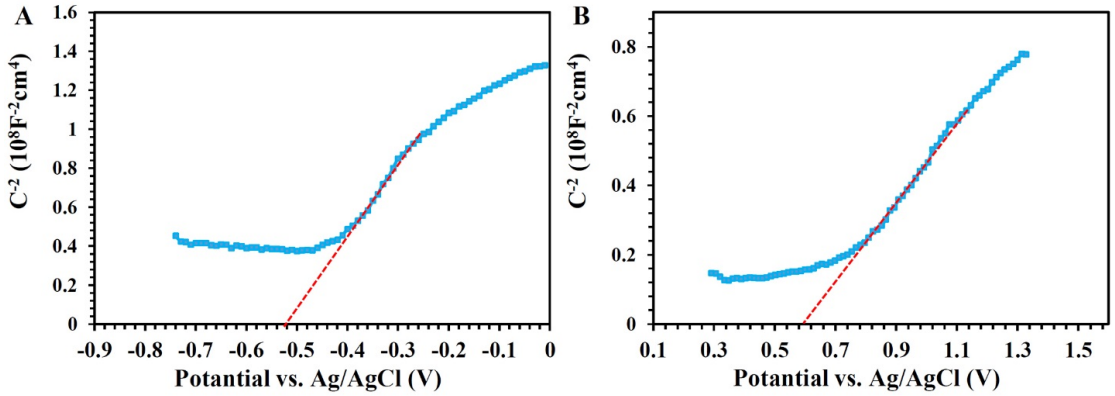

Fig. 5. Mott-Schottky measurements for (A) TiO_2 and (B) WO_3 samples.

Mott-Schottky

To determine the conduction and valance band energies of the TiO_2, and WO_3 samples, Mott-Schottky tests were conducted, as depicted in (Fig. 5). The Mott-Schottky curves of TiO_2 and WO_3 samples have positive slopes, reflecting that these samples are n-type semiconductors [45]. The flat band potentials (E_{FB}) for pure TiO_2 and WO_3 were found to be -0.52 and +0.6 V versus Ag/AgCl reference electrode (-0.32 and +0.5 V relative to NHE), respectively. It is generally documented that the conduction band potential (E_C) in n-type semiconductors is located ~0.1 eV lower than E_{FB}, and the potential of valance band (E_V) of p-type semiconductors is approximately 0.1 V higher than E_{FB} [46]. In this regard, the E_C of TiO_2 and WO_3 samples are calculated around -0.42 and +0.4 eV vs. NHE, respectively. Further, the E_V of TiO_2 and WO_3 samples are estimated through the equation $E_V=E_g + E_C$, and from the calculated E_C (from E_{FB}) and E_g (from DRS test and Tauc plots, Fig.3) therefore E_V of these samples is 2.68 and 3 eV vs. NHE, respectively.

Photocatalytic performance

The photocatalytic efficiencies of the prepared photocatalyst samples were examined by measuring the degradation percentage of Nitenpyram insecticide under visible light irradiation. Before irradiation, the adsorption on the surface of photocatalysts was studied in dark conditions, which results in a change in the Nitenpyram relative concentration (C/C_0) as the function of the processing time is shown in Fig. 6(A). As can be seen in this figure after 105 min, the adsorption stops for all samples, and the largest adsorption occurred for the TiO_2-WO_3 sample. As shown in Fig. 6(B), in the absence of any photocatalyst sample (Blank) the degradation of Nitenpyram is negligible while in the presence of TiO_2 and WO_3 samples, an impressive degradation of Nitenpyram has occurred. The TiO_2-WO_3 heterojunction photocatalyst has significantly improved photocatalytic performance, which can be attributed to the decrease of the charge carriers' recombination rate and improvement of the visible light absorbance. Because of the low concentration of Nitenpyram insecticide in the reaction solution, the apparent reaction rate constants (k_{app}) for its photocatalytic degradation reaction on the prepared samples were calculated from the Pseudo first-order reaction kinetic equation (Eq. (1)) according to the Langmuir-Hinshelwood [47].

$$\ln\left(\frac{C_0}{C_t}\right) = k_{app}t \qquad (1)$$

Where C_0 and C_t are the Nitenpyram concentrations at irradiation time (t) of 0 and t respectively. Fig. 6(C) shows the reaction kinetic curves for photocatalytic degradation of Nitenpyram over the prepared samples. k_{app} of the TiO_2, WO_3, and TiO_2-WO_3 samples are estimated as 0.0111, 0.0059, and 0.0312 min^{-1}, respectively.

In order to optimize the reaction condition for photocatalytic degradation of Nitenpyram over the TiO_2-WO_3 heterojunction nanocomposite under visible light irradiation, the reaction was repeated in the different photocatalyst concentrations and the different reaction solution pH. As seen in Fig. 7(A), maximum degradation is obtained at 300 ppm photocatalyst concentration. And according to the results of Fig. 7(B), the best performance is obtained at the reaction solution pH of 7. For

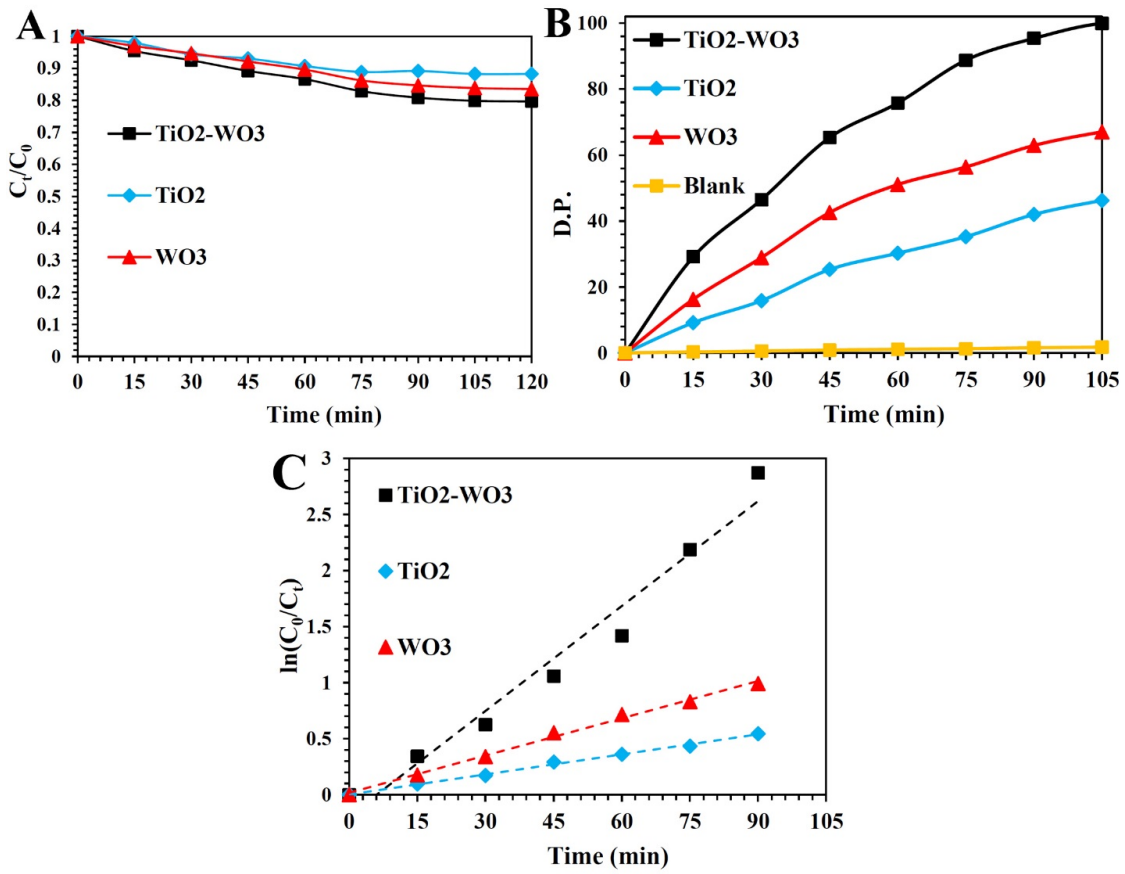

Fig. 6. (A) Change of the Nitenpyram relative concentration (C/C_0) as function of time during the adsorption process in dark condition, (B) Photocatalytic degradation percentage (D.P.) of Nitenpyram insecticide over the prepared samples under visible light irradiation and (C) Pseudo first-order reaction kinetics for Nitenpyram degradation over the prepared photocatalysts

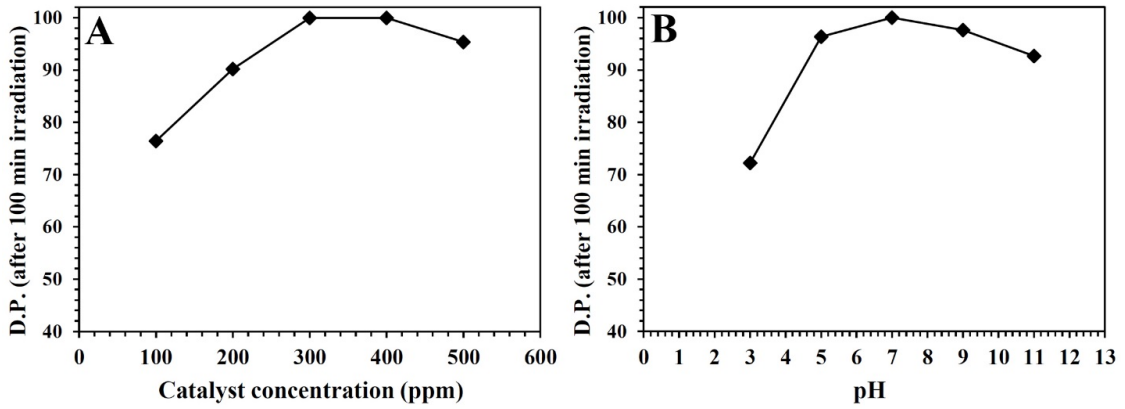

Fig.7. Degradation percentage (D.P.) of Nitenpyram insecticide over the TiO_2-WO_3 after 100 min visible light irradiation as function of (A) catalyst concentration (pH =7) and (B) pH of the reaction solution (catalyst concentration=300 ppm).

adjusting the reaction solution pH, aqueous solutions of HCl (0.01M) and NaOH (0.01M) were used. Therefore, the optimized reaction conditions are pH=7 and photocatalyst concentration=300 ppm.

In order to survey the stability of the TiO_2-WO_3 heterojunction nanocomposite during the photocatalytic degradation reaction, EDS and Raman analyses were performed before and after the degradation process, which results are shown

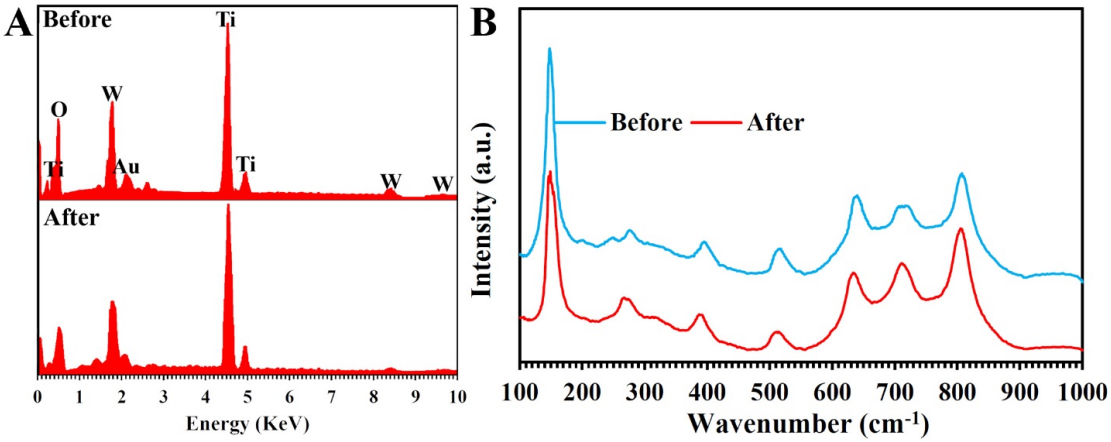

Fig.8. EDS (A) and Raman (B) spectra of the TiO_2-WO_3 sample before and after the degradation process.

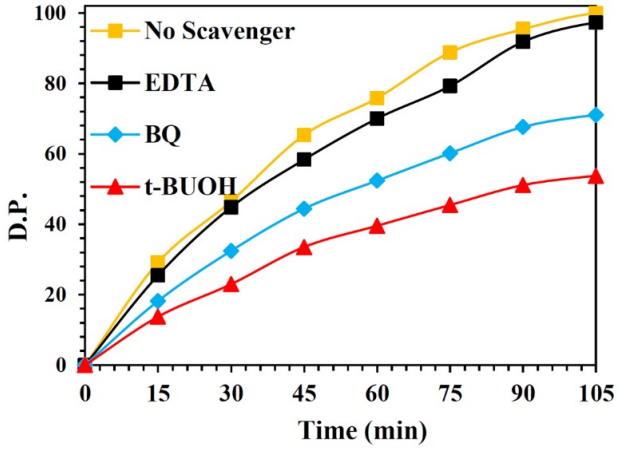

Fig. 9. Photocatalytic performance of TiO_2-WO_3 sample for degradation of Nitenpyram insecticide under visible light irradiation in presence of different scavengers.

in Fig. 8. As seen in Fig. 8(A), the peaks related to the O, Ti, and W elements, are seen in EDS spectra of the TiO_2-WO_3 nanocomposite, which indicates successful preparation of this heterojunction sample. Moreover, there is no obvious difference between the EDS spectra of the TiO_2-WO_3 sample before and after the degradation process, which confirms the good stability of the nanocomposite during the degradation reaction. In Raman spectra of the TiO_2-WO_3 heterojunction in Fig. 8(B), the peaks at wavenumbers of 149, 400, 521, and 640 cm^{-1} are indexed to Eg, B_{1g}, A_{1g} + $B_{1g,}$ and Eg modes of the anatase TiO_2, respectively [14], and the peaks at wavenumbers of 810 and 718 cm^{-1} are related to the stretching of O-W-O modes, and peaks at 136 and 276 cm^{-1} are attributed to the deformation of O-W-O modes WO_3 [48]. As observed in Fig. 8(B), there is no remarkable change in the Raman spectra of the TiO_2-WO_3 nanocomposite after the photocatalytic degradation reaction, which indicates acceptable stability of this heterojunction sample during the degradation process.

To further investigate the role of the active species during the photocatalytic decomposition of Nitenpyram insecticide on the TiO_2-WO_3 heterojunction, tert-Butyl alcohol (t-BUOH) as $OH^{\bullet}$ scavenger, benzoquinone (BQ) as $O_2^{\bullet-}$ scavenger, and Ethylenediaminetetraacetic acid (EDTA) as hole scavenger, with the concentration of 0.01 M was added to the photocatalytic reaction suspension in the optimum reaction conditions as mentioned in previous sections [49]. Fig.9 clearly indicates the highest decrease in the photocatalytic performance in presence of t-BUOH, which distinctly demonstrates the dominant role of $OH^{\bullet}$ radicals in photocatalytic

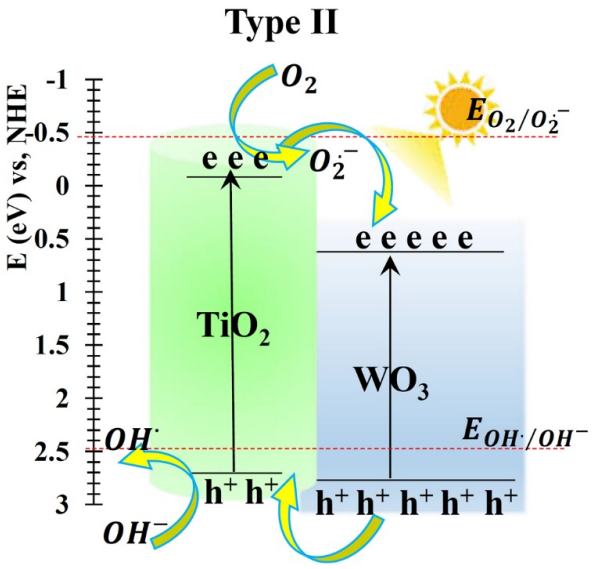

Fig. 10. Plausible type II charge transfer pathways for the photocatalytic activity of the TiO_2-WO_3 heterojunction.

degradation of Nitenpyram insecticide. Moreover, the photocatalytic activity is partially decreased in presence of BQ. In brief, the $OH^{\cdot}$ is the major cause of the photocatalytic degradation of Nitenpyram over the TiO_2-WO_3 nanocomposite under visible light irradiation.

Plausible type II charge transfer pathways for the photocatalytic activity of the TiO_2-WO_3 heterojunction are thoroughly discussed in Fig.10. In the type II mechanism, during the irradiation of the heterojunction photocatalyst, the electrons on the conduction band of TiO_2 migrate to the conduction band of WO_3, on the other hand, the photoinduced holes on the valence band of WO_3 migrate to the valence band TiO_2 [50]. In this regard, the charge carriers are efficiently separated and produce more $O_2^{\cdot-}$ and $OH^{\cdot}$ radicals. In this mechanism, the oxidation power of the photoinduced holes is improved, which results in the enhancement of the photocatalytic activity.

CONCLUSION

In summary, a novel TiO_2 nanorod/WO_3 nanoflakes heterojunction photocatalyst was synthesized from the combination of TiO_2 nanorod and WO_3 nanoflakes through an innovative hydrothermal technique and was applied for the first time for photocatalytic degradation of Nitenpyram insecticide under visible light irradiation. According to the obtained results, the highest photocatalytic efficiency was obtained for the TiO_2/WO_3 heterojunction sample with a photocatalytic reaction rate constant of 0.0312 min^{-1} which is 3 times higher than that of the pure TiO_2. The improved photocatalytic performance could be attributed to the decrease in the charge carrier's recombination rate and enhanced visible light harvesting. Moreover, based on the radical trapping experiments and Mott-Schottky calculations, the type II charge transfer pathway was suggested for the enhancement of the photocatalytic performance of the prepared heterojunction, and hydroxide radical was detected as the main active species for decomposition of Nitenpyram insecticide.

CONFLICT OF INTEREST

The authors declare no conflict of interest.

REFERENCES

[1] M. DiBartolomeis, S. Kegley, P. Mineau, R. Radford, K. Klein, An assessment of acute insecticide toxicity loading (AITL) of chemical pesticides used on agricultural land in the United States, PloS one, 14 (2019) e0220029. https://doi.org/10.1371/journal.pone.0220029

[2] J. Liu, W.H. Xiong, L.Y. Ye, W.S. Zhang, H. Yang, Developing a novel nanoscale porphyrinic metal-organic framework: A bifunctional platform with sensitive fluorescent detection and elimination of nitenpyram in agricultural environment, Journal of agricultural and food chemistry, 68 (2020) 5572-5578. https://doi.org/10.1021/acs.jafc.0c01313

[3] R. Priya, D. Ramesh, E. Khosla, Biodegradation of pesticides using density-based clustering on cotton crop affected by Xanthomonas malvacearum, Environment,

Development and Sustainability, 22 (2020) 1353-1369. https://doi.org/10.1007/s10668-018-0251-7

[4] L.F. Dumée, J.W. Maina, A. Merenda, R. Reis, L. He, L. Kong, Hybrid thin film nano-composite membrane reactors for simultaneous separation and degradation of pesticides, Journal of membrane science, 528 (2017) 217-224. https://doi.org/10.1016/j.memsci.2017.01.041

[5] N. Narayanan, S. Gupta, V.T. Gajbhiye, Decontamination of pesticide industrial effluent by adsorption-coagulation-flocculation process using biopolymer-nanoorganoclay composite, International Journal of Environmental Science and Technology, 17 (2020) 4775-4786. https://doi.org/10.1007/s13762-020-02785-y

[6] R. Wang, J. Pan, M. Qin, T. Guo, Molecularly imprinted nanocapsule mimicking phosphotriesterase for the catalytic hydrolysis of organophosphorus pesticides, European Polymer Journal, 110 (2019) 1-8. https://doi.org/10.1016/j.eurpolymj.2018.10.045

[7] A.P. Bhat, P.R. Gogate, Degradation of nitrogen-containing hazardous compounds using advanced oxidation processes: A review on aliphatic and aromatic amines, dyes, and pesticides, Journal of Hazardous Materials, 403 (2021) 123657. https://doi.org/10.1016/j.jhazmat.2020.123657

[8] A.G. Akerdi, S.H. Bahrami, Application of heterogeneous nano-semiconductors for photocatalytic advanced oxidation of organic compounds: a review, Journal of Environmental Chemical Engineering, 7 (2019) 103283. https://doi.org/10.1016/j.jece.2019.103283

[9] S.-Y. Lee, S.-J. Park, TiO2 photocatalyst for water treatment applications, Journal of industrial and engineering chemistry, 19 (2013) 1761-1769. https://doi.org/10.1016/j.jiec.2013.07.012

[10] Z. Xing, J. Zhang, J. Cui, J. Yin, T. Zhao, J. Kuang, Z. Xiu, N. Wan, W. Zhou, Recent advances in floating TiO2-based photocatalysts for environmental application, Applied Catalysis B: Environmental, 225 (2018) 452-467. https://doi.org/10.1016/j.apcatb.2017.12.005

[11] P.S. Basavarajappa, S.B. Patil, N. Ganganagappa, K.R. Reddy, A.V. Raghu, C.V. Reddy, Recent progress in metal-doped TiO2, non-metal doped/codoped TiO2 and TiO2 nanostructured hybrids for enhanced photocatalysis, International Journal of Hydrogen Energy, 45 (2020) 7764-7778. https://doi.org/10.1016/j.ijhydene.2019.07.241

[12] J.-J. Zhang, S.-S. Fang, J.-Y. Mei, G.-P. Zheng, X.-C. Zheng, X.-X. Guan, High-efficiency removal of rhodamine B dye in water using g-C3N4 and TiO2 co-hybridized 3D graphene aerogel composites, Separation and Purification Technology, 194 (2018) 96-103. https://doi.org/10.1016/j.seppur.2017.11.035

[13] S. Xue, H. Li, F. Cao, Y. Cao, X. Yue, Preparation of g-C3N4(Ag)/Gr/TiO2 Z-scheme photocatalyst with enhanced reduction property and the efficient degradation of rhodamine B, Journal of Alloys and Compounds, 898 (2022) 162759. https://doi.org/10.1016/j.jallcom.2021.162759

[14] G. Hosseinzadeh, N. Ghasemian, S. Zinatloo-Ajabshir, TiO2/graphene nanocomposite supported on clinoptilolite nanoplate and its enhanced visible light photocatalytic activity, Inorganic Chemistry Communications, 136 (2022) 109144. https://doi.org/10.1016/j.inoche.2021.109144

[15] W. Zhao, M. Adeel, P. Zhang, P. Zhou, L. Huang, Y. Zhao, S. Noman, M.A. Ahmad, B. Lou, Y. Jiang, A critical review on surface modified nano-catalysts application for photocatalytic degradation of volatile organic compounds, Environmental Science: Nano, (2022). https://doi.org/10.1039/D1EN00955A

[16] S. Al Jitan, G. Palmisano, C. Garlisi, Synthesis and surface modification of TiO2-based photocatalysts for the conversion of CO2, Catalysts, 10 (2020) 227. https://doi.org/10.3390/catal10020227

[17] A. Meng, L. Zhang, B. Cheng, J. Yu, Dual cocatalysts in TiO2 photocatalysis, Advanced Materials, 31 (2019) 1807660. https://doi.org/10.1002/adma.201807660

[18] B.T. Barrocas, N. Ambrožová, K. Kočí, Photocatalytic Reduction of Carbon Dioxide on TiO2 Heterojunction Photocatalysts-A Review, Materials, 15 (2022) 967. https://doi.org/10.3390/ma15030967

[19] H. Yang, A short review on heterojunction photocatalysts: Carrier transfer behavior and photocatalytic mechanisms, Materials Research Bulletin, 142 (2021) 111406. https://doi.org/10.1016/j.materresbull.2021.111406

[20] A. Bahadoran, M. Farhadian, G. Hoseinzadeh, Q. Liu, Novel flake-like Z-Scheme Bi2WO6-ZnBi2O4 heterostructure prepared by sonochemical assisted hydrothermal procedures with enhanced visible-light photocatalytic activity, Journal of Alloys and Compounds, 883 (2021) 160895. https://doi.org/10.1016/j.jallcom.2021.160895

[21] V. Dutta, S. Sharma, P. Raizada, V.K. Thakur, A.A.P. Khan, V. Saini, A.M. Asiri, P. Singh, An overview on WO3 based photocatalyst for environmental remediation, Journal of Environmental Chemical Engineering, 9 (2021) 105018. https://doi.org/10.1016/j.jece.2020.105018

[22] J. Murillo-Sierra, A. Hernández-Ramírez, L. Hinojosa-Reyes, J. Guzmán-Mar, A review on the development of visible light-responsive WO3-based photocatalysts for environmental applications, Chemical Engineering Journal Advances, 5 (2021) 100070. https://doi.org/10.1016/j.ceja.2020.100070

[23] X. Zhang, Y. Wei, R. Yu, Multidimensional Tungsten Oxides for Efficient Solar Energy Conversion, Small Structures, 3 (2022) 2100130. https://doi.org/10.1002/sstr.202100130

[24] R.S. Mim, E.S. Aldeen, A. Alhebshi, M. Tahir, Recent advancements in strategies to improve performance of tungsten-based semiconductors for photocatalytic hydrogen production: a review, Journal of Physics D: Applied Physics, (2021). https://doi.org/10.1088/1361-6463/ac21fc

[25] G. Yang, X. Zhu, G. Cheng, R. Chen, J. Xiong, W. Li, Y. Wei, Engineered tungsten oxide-based photocatalysts for CO 2 reduction: Categories and roles, Journal of Materials Chemistry A, 9 (2021) 22781-22809. https://doi.org/10.1039/D1TA04969K

[26] O. Samuel, M.H.D. Othman, R. Kamaludin, O. Sinsamphanh, H. Abdullah, M.H. Puteh, T.A. Kurniawan, WO3-based photocatalysts: A review on synthesis, performance enhancement and photocatalytic memory for environmental applications, Ceramics International, (2021). https://doi.org/10.1016/j.ceramint.2021.11.158

[27] J. Chen, X. Xiao, Y. Wang, Z. Ye, Fabrication of hierarchical sheet-on-sheet WO3/g-C3N4 composites with enhanced photocatalytic activity, Journal of Alloys and Compounds, 777 (2019) 325-334. https://doi.org/10.1016/j.jallcom.2018.10.404

[28] V. Ramar, K. Balasubramanian, Reduced Graphene Oxide/WO3 Nanorod Composites for Photocatalytic Degradation of Methylene Blue under Sunlight

Irradiation, ACS Applied Nano Materials, (2021). https://doi.org/10.1021/acsanm.1c00863
[29] Y. Liu, Y. Li, W. Li, S. Han, C. Liu, Photoelectrochemical properties and photocatalytic activity of nitrogen-doped nanoporous WO3 photoelectrodes under visible light, Applied Surface Science, 258 (2012) 5038-5045. https://doi.org/10.1016/j.apsusc.2012.01.080
[30] F. Mehmood, J. Iqbal, M. Ismail, A. Mehmood, Ni doped WO3 nanoplates: an excellent photocatalyst and novel nanomaterial for enhanced anticancer activities, Journal of Alloys and Compounds, 746 (2018) 729-738. https://doi.org/10.1016/j.jallcom.2018.01.409
[31] M. Farhadian, P. Sangpour, G. Hosseinzadeh, Morphology dependent photocatalytic activity of WO3 nanostructures, Journal of Energy Chemistry, 24 (2015) 171-177. https://doi.org/10.1016/S2095-4956(15)60297-2
[32] F. Siddique, S. Gonzalez-Cortes, T. Xiao, M.A. Rafiq, P.P. Edwards, Effect of surface modification and H2 reduction of WO3 nanoparticles in Methylene Blue photodegradation, Surface Topography: Metrology and Properties, 8 (2020) 045012. https://doi.org/10.1088/2051-672X/abbcb7
[33] M.G. Peleyeju, E.L. Viljoen, WO3-based catalysts for photocatalytic and photoelectrocatalytic removal of organic pollutants from water-A review, Journal of Water Process Engineering, 40 (2021) 101930. https://doi.org/10.1016/j.jwpe.2021.101930
[34] B. Basumatary, R. Basumatary, A. Ramchiary, D. Konwar, Evaluation of Ag@ TiO2/WO3 heterojunction photocatalyst for enhanced photocatalytic activity towards organic pollutant, Chemosphere, (2021) 131848. https://doi.org/10.1016/j.chemosphere.2021.131848
[35] A. Dehdar, G. Asgari, M. Leili, T. Madrakian, A. Seid-Mohammadi, Step-scheme BiVO4/WO3 heterojunction photocatalyst under visible LED light irradiation removing 4-chlorophenol in aqueous solutions, Journal of Environmental Management, 297 (2021) 113338. https://doi.org/10.1016/j.jenvman.2021.113338
[36] L. He, S. Zhang, J. Zhang, G. Chen, S. Meng, Y. Fan, X. Zheng, S. Chen, Investigation on the Mechanism and Inner Impetus of Photogenerated Charge Transfer in WO3/ZnO Heterojunction Photocatalysts, The Journal of Physical Chemistry C, 124 (2020) 27916-27929. https://doi.org/10.1021/acs.jpcc.0c08860
[37] Y.-L. Wei, B. Rong, X. Chen, Y.-Y. Ding, Y.-F. Huang, L.-Q. Fan, J.-H. Wu, Porous and visible-light-driven p-n heterojunction constructed by Bi2O3 nanosheets and WO3 microspheres with enhanced photocatalytic performance, Separation and Purification Technology, 256 (2021) 117815. https://doi.org/10.1016/j.seppur.2020.117815
[38] F. Puga, J.A. Navío, M.C. Hidalgo, Features of coupled AgBr/WO3 materials as potential photocatalysts, Journal of Alloys and Compounds, 867 (2021) 159191. https://doi.org/10.1016/j.jallcom.2021.159191
[39] M.R.S. Joice, T.M. David, P. Wilson, WO3 nanorods supported on mesoporous TiO2 nanotubes as one-dimensional nanocomposites for rapid degradation of methylene blue under visible light irradiation, The Journal of Physical Chemistry C, 123 (2019) 27448-27464. https://doi.org/10.1021/acs.jpcc.9b05647
[40] V. Puddu, R. Mokaya, G.L. Puma, Novel one step hydrothermal synthesis of TiO 2/WO 3 nanocomposites with enhanced photocatalytic activity, Chemical communications, (2007) 4749-4751. https://doi.org/10.1039/b711559h
[41] X. Zheng, S. Das, Y. Gu, S. Liu, J. Zhao, Optimal engineering of CdS/PbS co-sensitized TiO2 nanotube arrays for enhanced photoelectrochemical performance, Ceramics International, 46 (2020) 12050-12058. https://doi.org/10.1016/j.ceramint.2020.01.246
[42] M. Ikram, S. Rasheed, A.M. Afzal, N.A. Shad, Y. Javed, A. Mohyuddin, T. Alomayri, M.M. Sajid, A. Almahri, D. Hussain, Ultrasensitive V doped WO3 1D nanorods heterojunction photodetector with pronounced photosensing activities, Journal of Alloys and Compounds, 909 (2022) 164753. https://doi.org/10.1016/j.jallcom.2022.164753
[43] Y. Lin, S. Wu, X. Li, X. Wu, C. Yang, G. Zeng, Y. Peng, Q. Zhou, L. Lu, Microstructure and performance of Z-scheme photocatalyst of silver phosphate modified by MWCNTs and Cr-doped SrTiO3 for malachite green degradation, Applied Catalysis B: Environmental, 227 (2018) 557-570. https://doi.org/10.1016/j.apcatb.2018.01.054
[44] E. Radha, D. Komaraiah, R. Sayanna, J. Sivakumar, Photoluminescence and photocatalytic activity of rare earth ions doped anatase TiO2 thin films, Journal of Luminescence, 244 (2022) 118727. https://doi.org/10.1016/j.jlumin.2022.118727
[45] N. Son, J. Lee, T. Yoon, M. Kang, Design for a longer photoinduced charge separation and improved visible-light-driven H2 generation through structure reversal and oxygen vacancies via Ni substitution into ZnFe2O4 spinel, Ceramics International, 47 (2021) 20317-20334. https://doi.org/10.1016/j.ceramint.2021.04.040
[46] S. Das, S. Patnaik, K. Parida, Dynamic charge transfer through Fermi level equilibration in the p-CuFe 2 O 4/n-NiAl LDH interface towards photocatalytic application, Catalysis Science & Technology, 10 (2020) 6285-6298. https://doi.org/10.1039/D0CY00980F
[47] F. Akhlaghian, A. Najafi, CuO/WO3/TiO2 photocatalyst for degradation of phenol wastewater, Scientia Iranica, 25 (2018) 3345-3353. https://doi.org/10.24200/sci.2018.20611
[48] M. Daniel, B. Desbat, J. Lassegues, B. Gerand, M. Figlarz, Infrared and Raman study of WO3 tungsten trioxides and WO3, xH2O tungsten trioxide tydrates, Journal of solid state chemistry, 67 (1987) 235-247. https://doi.org/10.1016/0022-4596(87)90359-8
[49] Q. Wang, S. Zhu, S. Zhao, C. Li, R. Wang, D. Cao, G. Liu, Construction of Bi-assisted modified CdS/TiO2 nanotube arrays with ternary S-scheme heterojunction for photocatalytic wastewater treatment and hydrogen production, Fuel, 322 (2022) 124163. https://doi.org/10.1016/j.fuel.2022.124163
[50] D. Kim, K. Yong, Boron doping induced charge transfer switching of a C3N4/ZnO photocatalyst from Z-scheme to type II to enhance photocatalytic hydrogen production, Applied Catalysis B: Environmental, 282 (2021) 119538. https://doi.org/10.1016/j.apcatb.2020.119538